Inorg. Chem. **2003**, *42*, 5192–5201

Electrical Conducting and Magnetic Properties of (Ethylenedithiotetrathiafulvalenothioquinone-1,3-diselenolemethide)$_2$·FeBr$_4$ (GaBr$_4$) Crystals with Two Different Interlayer Arrangements of Donor Molecules

Takuya Matsumoto,[†] Yohsuke Kamada,[†] Toyonari Sugimoto,*[,†,‡] Toshiji Tada,[†,‡] Satoru Noguchi,[§] Hiroyuki Nakazumi,[§] Motoo Shiro,[||] Harukazu Yoshino,[⊥] and Keizo Murata[⊥]

Research Institute for Advanced Science and Technology, Osaka Prefecture University, Osaka 599-8570, Japan, CREST, Japan and Technology Corporation, Saitama 332-0012, Japan, Graduate School of Engineering, Osaka Prefecture University, Osaka 599-8531, Japan, Rigaku Corporation, Tokyo 196-8666, Japan, and Graduate School of Science, Osaka City University, Osaka 558-8585, Japan

Received March 3, 2003

Two donor molecules newly synthesized, dimethylthio- and ethylenedithio-tetrathiafulvalenothioquinone-1,3-diselenolemethides (**1** and **2**), were used to prepare their charge-transfer (CT) salts with a magnetic $FeBr_4^-$ counteranion. For **1**, a low electrical conducting 1:1 salt (**1**·$FeBr_4$) was obtained, in which molecules of **1** are tightly dimerized in a one-dimensional (1D) stacking column. On the other hand, **2** gave a 2:1 salt (**2**$_2$·$FeBr_4$) as two different kinds of plate crystals (**I** and **II**). Both **I** and **II** possess similar stacking structures of molecules of **2** in each 1D column with a half-cut pipelike structure along the *c* axis. However, for **I**, the stacking columns are aligned in the same direction along the *a* and *b* axes, while for **II** they are in the same direction along the *a* axis, but in the reverse direction along the *b* axis, resulting in the difference in the relative arrangement of molecules of **2** and $FeBr_4^-$ ions between the two crystals. The room-temperature electrical conductivities of the single crystals of **I** and **II** were 13.6 and 12.7 S cm^{-1}, respectively. The electrical conducting behavior in **I** was metallic above 170 K but changed to be semiconducting with a very small activation energy of 7.0 meV in the temperature range 4–170 K. In contrast, **II** showed the semiconducting behavior in the whole temperature range 77–285 K. The corresponding nonmagnetic $GaBr_4^-$ salts with almost the same crystal structure as **I** and **II** showed definitively different electrical conducting properties in the metal to semiconductor transition temperature in **I** as well as in the magnitude of activation energy in the semiconducting region of **I** and **II**. The interaction between the d spins of $FeBr_4^-$ ions was weak and antiferromagnetic in both **I** and **II**, but the magnitude of the spin interaction was unexpectedly larger compared with that in the $FeBr_4^-$ salt of the corresponding sulfur derivative of **2** with closer contact between the neighboring $FeBr_4^-$ ions. These electrical conducting and magnetic results suggest a significant interaction between the conducting π electrons and the d spins of $FeBr_4^-$ ions located near the columns or layers.

Introduction

Molecular π/d systems based on charge-transfer (CT) salts of several donor molecules with magnetic metal counteranions[1] have so far been discovered, which exhibit paramagnetism/superconductivity,[2−4] metamagnetism/superconductivity,[5,6] ferromagnetism/metallic conductivity,[7] and a high

* To whom correspondence should be addressed. E-mail: toyonari@riast.osakafu-u.ac.jp.
[†] Research Institute for Advanced Science and Technology, Osaka Prefecture University.
[‡] CREST, Japan and Technology Corporation.
[§] Graduate School of Engineering, Osaka Prefecture University.
[||] Rigaku Corporation.
[⊥] Osaka City University.

(1) Day, P. *Philos. Trans. R. Soc. London, Ser. A* **1985**, *145*, 314.
(2) Graham, A. W.; Kurmoo, M.; Day, P. *J. Chem. Soc., Chem. Commun.* **1995**, 2061.
(3) Kurmoo, M.; Graham, A. W.; Day, P.; Coles, S. J.; Hursthouse, M. B.; Caulfield, J. L.; Singleton, J.; Pratt, F. L.; Hayes, W.; Ducasse, L.; Guionneau, P. *J. Am. Chem. Soc.* **1995**, *117*, 12209.
(4) Martin L.; Turner, S. S.; Day, P.; Mabbs, F. E.; McInnes, E. J. L. *Chem. Commun.* **1997**, 1367.

10.1021/ic030083v CCC: $25.00
Published on Web 07/22/2003

magnetic field-induced ferromagnetism/superconductivity.[8,9] Nevertheless, a lot of efforts still continue to be made for searching for new molecular π/d systems, in which conducting π electrons and localized d spins significantly interact with each other so as to produce unique and cooperative electrical conducting and magnetic properties at moderate temperature and normal pressure.

We now prepared CT salts of new donor molecules of dimethylthio- and ethylenedithio-tetrathiafulvalenothioquinone-1,3-diselenolemethides (**1** and **2**), selenium analogues of their corresponding 1,3-dithiole compounds (**3** and **4**) already synthesized in our laboratory[10,11] with magnetic $FeBr_4^-$ and nonmagnetic $GaBr_4^-$ counteranions, and investigated a possibility of π/d interaction in the $FeBr_4^-$ salts by comparison of crystal structures and electrical conducting/magnetic properties between the $FeBr_4^-$ and $GaBr_4^-$ salts. In our previous study, **3** and **4** gave only 1:1 CT salts with $FeBr_4^-$ ion, whose room-temperature electrical conductivities were quite low.[12] However, in the use of a carbonyl analogue of **4**, ethylenedithiotetrathiafulvalenoquinone-1,3-dithiolemethide (**5**), a highly conducting 2:1 CT salt with $FeBr_4^-$ ion ($\mathbf{5}_2$·$FeBr_4$) was obtained as plate[13] and needle crystals,[14] of which the needle crystal exhibited metallic conductivity above 170 K and very interestingly ferromagnetic interaction between the d spins of $FeBr_4^-$ ions by participation of the conducting π electrons below ca. 15 K. Since very recent preliminary results indicate a possibility of ferromagnetic ordering below 1 K,[15] indeed this needle crystal generates much expectation for the opening of a new research area of "molecular spintronics" based on the molecular π/d systems.[16−18]

To this end, there remains an unavoidable task of preparing molecular ferromagnetic semiconductors or metals working at temperatures as high as possible by making the π/d interaction increase markedly. We planned to synthesize new donor molecules, in which S atoms residing in **3**, **4**, and **5**

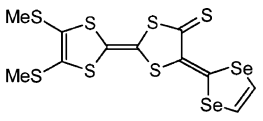

1

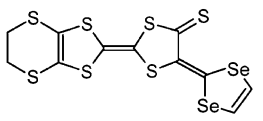

2

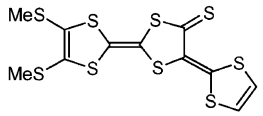

3

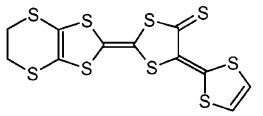

4

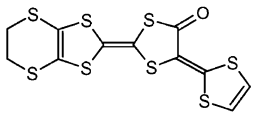

5

are all or partially replaced by Se atoms, since contacts between the Se atoms of such a donor molecule and the Br atoms of $FeBr_4^-$ ion will become much closer, if the crystal structures of $FeBr_4^-$ salts have only a minor change. For such a first step, **1** and **2** were successfully synthesized and used for the preparation of their $FeBr_4^-$ and $GaBr_4^-$ salts. Especially, for **2**, each 2:1 CT salt with $FeBr_4^-$ or $GaBr_4^-$ ion ($\mathbf{2}_2$·$FeBr_4$ and $\mathbf{2}_2$·$GaBr_4$) was obtained as two different kinds of plate crystals (**I** and **II**). Irrespective of $FeBr_4^-$ and $GaBr_4^-$ counteranions, both **I** and **II** have similar one-dimensional (1D) stacking columns of molecules of **2** with a half-cut pipelike structure along the *c* axis, but for **I**, the stacking columns are aligned in the same direction along the *a* and *b* axes, while for **II** in the same direction along the *a* axis and in the reverse direction along the *b* axis. Very interestingly, **I** was metallic above 170 K and semiconducting below 170 K, while **II** was semiconducting in the whole temperature range measured. This is the first observation of marked change in the electrical conducting behavior by different arrangement of π-stacked layers. From comparison of electrical conducting and magnetic properties between $\mathbf{2}_2$·$FeBr_4$ (**I**) and $\mathbf{2}_2$·$GaBr_4$ (**I**), and between $\mathbf{2}_2$·$FeBr_4$ (**II**) and $\mathbf{2}_2$·$GaBr_4$ (**II**), it is most probable that significant interaction occurs between the conducting π electrons on the **2**-stacked columns or layers and the d spins of neighboring $FeBr_4^-$ ions in $\mathbf{2}_2$·$FeBr_4$ (**I**) and $\mathbf{2}_2$·$FeBr_4$ (**II**).

Experimental Section

Synthesis of 1, 2, 1·$FeBr_4$, $\mathbf{2}_2$·$FeBr_4$ (I, II), and $\mathbf{2}_2$·$GaBr_4$ (I, II). Bis(tetraethylammonium) bis[(2,3-dimethylthio- or 2,3-ethylenedithio-tetrathiafulvalenyl-6,7-dithiolato)zinc] complex[19] was reacted with 5 equiv of 2-methylseleno-1,3-diselenolanium tetrafluoroborate[20] in THF/DMF (1:1) at room temperature under argon for 8 h. After separation of the reaction mixture by column chromatography on silica gel, followed by recrystallization from CS_2/*n*-hexane, **1** and **2** were obtained as black crystals in 40% and

(5) Ojima, E.; Fujiwara, H.; Kato, K.; Kobayashi, H.; Tanaka, H.; Kobayashi, A.; Tokumoto, M.; Cassoux, P. *J. Am. Chem. Soc.* **1999**, *121*, 5581.
(6) Fujiwara, H.; Fujiwara, E.; Nakazawa, Y.; Narymbetov, B. Zh.; Kato, K.; Kobayashi, H.; Kobayashi, A.; Tokumoto, M.; Cassoux P. *J. Am. Chem. Soc.* **2001**, *123*, 306.
(7) Coronado, E.; Galán-Mascarós, J. R.; Gómez-Garcia, C. J.; Laukhin, V. *Nature* **2000**, *408*, 447.
(8) Uji, S.; Shinagawa, H.; Terashima, T.; Yakabe, T.; Tokumoto, M.; Kobayashi, A.; Tanaka, H.; Kobayashi, H. *Nature* **2001**, *410*, 908.
(9) Fujiwara, H.; Kobayashi, H.; Fujiwara, E.; Kobayashi, E. *J. Am. Chem. Soc.* **2002**, *124*, 6816.
(10) Iwamatsu, M.; Kominami, T.; Ueda, K.; Sugimoto, T.; Fujita, H.; Adachi, T. *Chem. Lett.* **1999**, 329.
(11) Iwamatsu, M.; Kominami, T.; Ueda, K.; Sugimoto, T.; Tada, T.; Nishimura, K.-i.; Adachi, T.; Fujita, H.; Guo, F.; Yokogawa, S.; Yoshino, H.; Murata, K.; Shiro, M. *J. Mater. Chem.* **2001**. *11*, 385.
(12) Kominami, T.; Matsumoto, T.; Ueda, K.; Sugimoto, T.; Murata, K.; Shiro, M.; Fujita, H. *J. Mater. Chem.* **2001**, *11*, 2089.
(13) Matsumoto, T.; Kominami, T.; Ueda, K.; Sugimoto, T.; Tada, T.; Yoshino, H.; Murata, K.; Shiro, M.; Negishi, E.; Matsui, H.; Toyota, N.; Endo, S.; Takahashi, K. *J. Solid State Chem.* **2002**, *168*, 408.
(14) Kominami, T.; Ueda, K.; Sugimoto, T.; Tada, T.; Noguchi, S.; Yoshino, H.; Murata, K.; Shiro, M.; Negishi, E.; Toyota, N.; Endo, S.; Takahashi, K. *Inorg. Chem.* **2002**, *41*, 4763.
(15) Noguchi, S.; Matsumoto, A.; Ishida, T.; Matsumoto, T.; Sugimoto, T.; Katori, H. Unpublished result.
(16) Prinz, G. A. *Science* **1998**, *282*, 1660.
(17) Ball, P. *Nature* **2000**, *404*, 918.
(18) Ohno, H. *Science* **2001**, *291*, 840.
(19) Ueda, K.; Yamanoha, M.; Sugimoto, T.; Fujita, H.; Ugawa, A.; Yakushi, K.; Kano, K. *Chem Lett.* **1997**, 461.
(20) Binet, L.; Fabre, J. M.; Montginoul, C.; Simonsen, K. B.; Becher, J. *J. Chem. Soc., Perkin Trans. 1* **1996**, 783.

37% yields, respectively. The **1**·$FeBr_4$, $\mathbf{2}_2$·$FeBr_4$ (**I**, **II**), and $\mathbf{2}_2$·$GaBr_4$ (**I**, **II**) salts were obtained by electrochemical oxidation of a chlorobenzene/ethanol (9:1, v/v) solution containing **1** or **2** (5.0 mg, 9.6×10^{-3} mmol) and NEt_4·$FeBr_4$ (48.5 mg, 9.6×10^{-2} mmol) or NEt_4·$GaBr_4$ (50.0 mg, 9.6×10^{-2} mmol) in a conventional H-shaped cell with Pt electrodes at 22 °C at a constant current of 0.3 μA. After about one week, the block crystals of **1**·$FeBr_4$ (mp > 300 °C) and the plate crystals of $\mathbf{2}_2$·$FeBr_4$ (**I, II**) (mp > 300 °C) and $\mathbf{2}_2$·$GaBr_4$ (**I, II**) (mp > 300 °C) were separated out the surface of the Pt electrode. Calcd for **1**·$FeBr_4$ ($C_{11}H_8S_7FeBr_4$): C, 14.71; H, 0.90. Found: C, 14.93; H, 0.78. Calcd for $\mathbf{2}_2$·$FeBr_4$ (**I**) ($C_{22}H_{12}S_{12}Se_4FeBr_4$): C, 18.65; H, 0.85. Found: C, 18.50; H,1.02. Calcd for $\mathbf{2}_2$·$FeBr_4$ (**II**) ($C_{22}H_{12}S_{12}Se_4FeBr_4$): C, 18.65; H, 0.85. Found: C, 18.56; H, 1.06. Calcd for $\mathbf{2}_2$·$GaBr_4$ (**I**) ($C_{22}H_{12}S_{12}Se_4GaBr_4$): C, 18.47; H, 0.85. Found: C, 18.35; H, 0.80. Calcd for $\mathbf{2}_2$·$GaBr_4$ (**II**) ($C_{22}H_{12}S_{12}Se_4GaBr_4$): C, 18.47; H, 0.85. Found: C, 18.19; H, 0.85.

X-ray Data Collection, Structure Solution, and Refinement. The X-ray diffraction data were collected at 296 or 93 K for the single crystals of **1**, **1**·$FeBr_4$, $\mathbf{2}_2$·$FeBr_4$ (**I**, **II**), and $\mathbf{2}_2$·$GaBr_4$ (**I**, **II**) on a Rigaku RAXIS-RAPID imaging plate diffractometer with graphite monochromated Mo Kα radiation ($\lambda = 0.71069$ Å). Table 1 shows their crystallographic data. The structures were solved by direct methods (SIR92,[21] SIR97,[22] and DIRDIF94[23]) and refined on F_o^2 with full-matrix least-squares analysis. Calculated positions of the hydrogen atoms [d(C − H) = 0.95 Å] were included in the final calculations. All the calculations were performed by using the teXsan crystallographic software package of the Molecular Structure Corporation.[24] For **1**, the final cycle of least-squares refinement on F_o^2 for 3013 data and 126 parameters converged to wR2(F_o^2) = 0.233 and R1 = 0.120 for all the data. For **1**·$FeBr_4$, the final cycle of least-squares refinement on F_0^2 for 5262 data and 198 parameters converged to wR2(F_0^2) = 0.168 for all the data and to R1 = 0.069 for 2298 data with $I \geq 3.00\sigma(I)$. For $\mathbf{2}_2$·$FeBr_4$ (**I**), the final cycle of least-squares refinement on F_o^2 for 7621 data and 405 parameters converged to wR2(F_o^2) = 0.092 and R1 = 0.047 for all the data. For $\mathbf{2}_2$·$FeBr_4$ (**II**), the final cycle of least-squares refinement on F_o^2 for 8831 data and 296 parameters converged to wR2(F_o^2) = 0.153 and R1 = 0.072 for all the data. For $\mathbf{2}_2$·$GaBr_4$ (**I**), the final cycle of least-squares refinement on F_o^2 for 9583 data and 405 parameters converged to wR2(F_o^2) = 0.107 and R1 = 0.048 for all the data. For $\mathbf{2}_2$·$GaBr_4$ (**II**), the final cycle of least-squares refinement on F_o^2 for 8866 data and 406 parameters converged to wR2(F_o^2) = 0.129 and R1 = 0.062 for all the data.

Electrical Conductivity, Magnetic Susceptibility, and ESR Measurements. Electrical conductivity was measured on each of the single crystals of **1**·$FeBr_4$, $\mathbf{2}_2$·$FeBr_4$ (**I**, **II**), and $\mathbf{2}_2$·$GaBr_4$ (**I**, **II**) using a four-probe method in the temperature range 5−300 or 77−285 K. The contact to the electrode was performed with gold paste. The magnetization at different temperatures between 1.8 and 300 K was measured using the microcrystals of **1**·$FeBr_4$ and $\mathbf{2}_2$·$FeBr_4$ (**I**, **II**) under an applied field of 1 kOe with a SQUlD magnetometer (MPMS XL, Quantum Design). The magnetic susceptibility (χ_{obs}) was obtained by dividing the observed magnetization with the applied field used. The paramagnetic susceptibility (χ_p) was obtained by subtracting the diamagnetic contribution calculated by a Pascal method[25] from χ_{obs}. The ESR spectra of the microcrystals of $\mathbf{2}_2$·$FeBr_4$ (**I**, **II**) and $\mathbf{2}_2$·$GaBr_4$ (**I**, **II**) were recorded with a frequency of 9.46672 GHz using a Bruker ESP-300E spectrometer. The g value was determined using a gaussmeter.

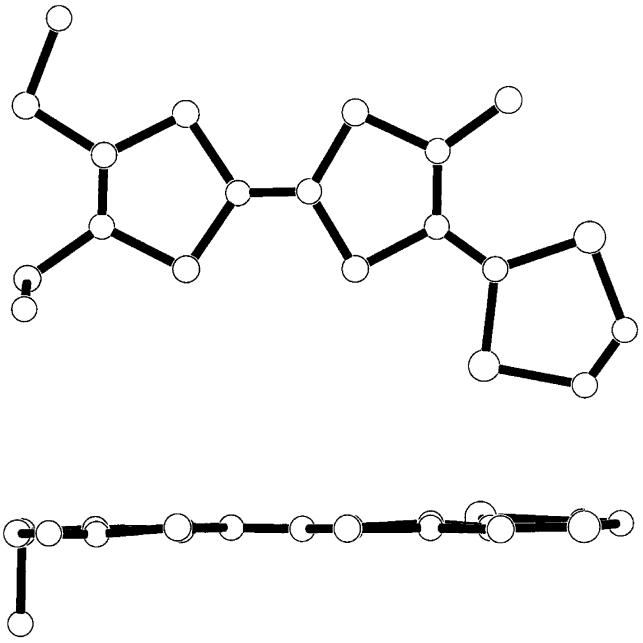

Figure 1. Molecular structure of **1**.

Results and Discussion

Molecular Structures, Redox Properties, and HOMOs of 1 and 2. In Figure 1, the molecular structure of **1** is shown, whose molecular skeleton except for the two methyl groups is almost planar, although the bending angle (4.19°) between the tetrathiafulvalenothioquinone and 1,3-diselenole rings is slightly larger than that (1.0°) between the two five-membered rings in the tetrathiafulvalenothioquinone ring. The distance of the C═S bond is 1.66 Å, which is the same to that of the corresponding 1,3-dithiole analogue (**3**).[10] Unfortunately, despite a lot of attempts, the single crystal of **2** has not yet been successfully obtained such that it is suitable for the X-ray structure analysis.

In each of the cyclic voltammograms of **1** and **2** measured in DMF at 0 °C, two pairs of reversible redox waves were observed, which are due to electron transfer processes between **1** (**2**) and their radical cations ($\mathbf{1}^{+\bullet}$ and $\mathbf{2}^{+\bullet}$), and between $\mathbf{1}^{+\bullet}$ ($\mathbf{2}^{+\bullet}$) and their dications, respectively. The redox potentials are +0.62 and +0.78 V versus Ag/AgCl for **1**, and +0.62 and +0.77 V for **2**, and very close to those (+0.64/+0.80 and +0.64/+0.81 V) of **3**[10] and the corresponding 1,3-dithiole analogue of **2** (**4**).[11] This can be readily understood by comparing the HOMOs of **1** (**2**) and **3** (**4**) with each other. The HOMO energies of **1**, **2**, **3**, and **4** calculated by a MOPAC method[26] are −6.947, −6.611,

(21) Altomare, A.; Burlea, M. C.; Gamalli, M.; Cascarano, G. L.; Giacovazzo, C.; Guagliardi, A.; Polidre, G. *J. Appl. Crystallogr*. **1994**, *27*, 435.
(22) Altomare, A.; Burlea, M. C.; Gamalli, M.; Cascarano, G. L.; Giacovazzo, C.; Guagliardi, A.; Moliterni, A. G. G.; Polidre, G.; Spagna, R. *J. Appl. Crystallogr*. **1999**, *32*, 115.
(23) Beurskens, P. T.; Admiraal, G.; Beurskens, G.; Bosman, W. P.; de Gelder, D.; Israel, R.; Smith, J. M. M. In *Technical Report of the Crystallography Laboratory*; University of Nijmegen: The Netherlands, 1994.
(24) *TeXsan, Crystal Structure Analysis Package*; Molecular Structure Corporation: Houston, TX, 1985 and 1992.
(25) König, E. *Landolt-Bornstein, Group II: Atomic and Molecular Physics, Vol. 2, Magnetic Properties of Coordination and Organometallic Transition Metal Compounds*; Springer-Verlag: Berlin, 1966.

Table 1. Crystallographic Data for **1**, **1**·$FeBr_4$, $\mathbf{2}_2$·$FeBr_4$ (**I**), $\mathbf{2}_2$·$GaBr_4$ (**I**), $\mathbf{2}_2$·$FeBr_4$ (**II**), and $\mathbf{2}_2$·$GaBr_4$ (**II**)

	1	**1**·$FeBr_4$	$\mathbf{2}_2$·$FeBr_4$ (**I**)	$\mathbf{2}_2$·$GaBr_4$ (**I**)	$\mathbf{2}_2$·$FeBr_4$ (**II**)	$\mathbf{2}_2$·$GaBr_4$ (**II**)
formula	$C_{11}H_8S_7Se_2$	$(C_{11}H_8S_7Se_2)$·$FeBr_4$	$(C_{11}H_6S_7Se_2)_2$·$FeBr_4$	$(C_{11}H_6S_7Se_2)_2$·$GaBr_4$	$(C_{11}H_6S_7Se_2)_2$·$FeBr_4$	$(C_{11}H_6S_7Se_2)_2$·$GaBr_4$
M_r	522.52	897.99	1416.48	1430.35	1416.48	1430.35
cryst size (mm)	0.40 × 0.05 × 0.005	0.15 × 0.10 × 0.05	0.25 × 0.10 × 0.01	0.30 × 0.08 × 0.01	0.25 × 0.10 × 0.01	0.30 × 0.04 × 0.01
cryst habit	black platelet	black block	black platelet	black platelet	black platelet	black platelet
cryst syst	monoclinic	triclinic	monoclinic	monoclinic	monoclinic	monoclinic
space group	$P2_1/n$	$P\bar{1}$	Pc	Pc	$P2_1/c$	$P2_1/c$
a (Å)	11.34(1)	8.721(2)	7.318(2)	7.307(2)	7.538(3)	7.512(3)
b (Å)	28.08(3)	10.422(2)	19.066(5)	19.132(6)	37.45(1)	37.59(1)
c (Å)	5.193(5)	14.181(2)	14.128(4)	14.166(5)	14.070(4)	14.073(3)
α (deg)	90	69.300(9)	90	90	90	90
β (deg)	96.36(4)	75.958(3)	97.69(2)	98.23(3)	103.14(3)	103.37(3)
γ (deg)	90	83.227(7)	90	90	90	90
cell volume (Å^3)	1643(3)	1168.8(3)	1953.5(9)	1959(1)	3867(2)	3866(2)
Z	4	2	2	2	4	4
temp (K)	296	296	93	93	93	93
ρ (g cm^{-3})	2.111	2.551	2.408	2.424	2.432	2.457
μ(Mo Kα) (cm^{-1})	53.73	112.39	89.85	92.73	90.76	90.76
$2\theta_{max}$	55.0	55.0	55.0	55.0	55.0	55.0
voltage, current	56 kV, 40 mV	56 kV, 40 mV	60 kV, 90 mV	60 kV, 90 mV	60 kV, 90 mV	60 kV, 90 mV
scan type	ω	ω	ω	ω	ω	ω
unique data	3013	5262	7621	9583	8831	8866
R_{merge}	0.13	0.04	0.09	0.09	0.15	0.11
weighting scheme	$1/\sigma^2(F_o^2)$	$1/\sigma^2(F_o^2)$	$1/\sigma^2(F_o^2)$	$1/\sigma^2(F_o^2)$	$1/\sigma^2(F_o^2)$	$1/\sigma^2(F_o^2)$
residual electron density (min, max) (e Å^{-3})	−3.49, 3.76	−1.26, 2.90	−1.08, 1.19	0.00, 1.03	0.00, 1.23	−1.92, 3.06
no. params refined	126	198	405	405	296	406
R1[a]	0.120	0.069	0.047	0.048	0.072	0.062
wR2[b]	0.233	0.168	0.092	0.107	0.153	0.129

[a] $R_1 = (\sum||F_o| - |F_c||)/(\sum|F_o|)$. [b] $wR2 = [\Sigma w(F_o^2 - F_c^2)^2/\Sigma w(F_o^2)^2]^{1/2}$.

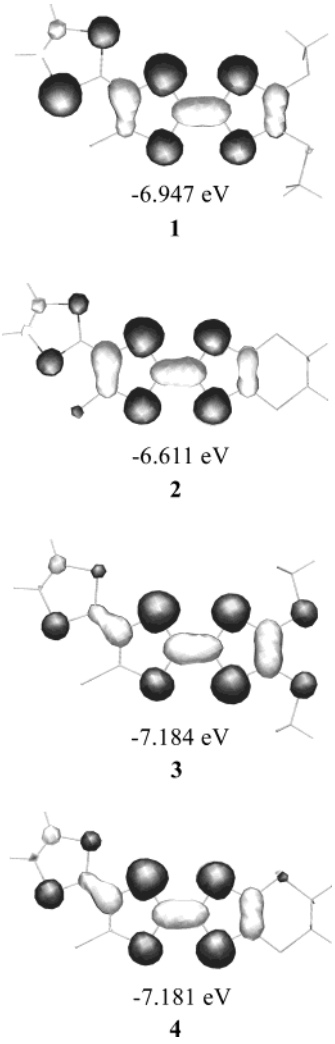

Figure 2. Energies and AO distribution in the HOMOs of **1**, **2**, **3**, and **4**.

−7.184, and −7.181 eV, respectively, which are compatible with the tendency of their first redox potentials observed. On the other hand, as the atomic orbital (AO) distributions in the HOMOs of **2** and **3** show in Figure 2, in both cases the AO coefficients are large at the central tetrathiaethylene moiety and moderate at the C═C bond. However, **2** and **3** have very different distributions of AOs in the (1,3-dithiole-2-ylidenyl)thione moiety. Thus, in **2** the AOs have small coefficients at the other positions as compared to one C atom of a 1,3-dithiole ring and both C and S atoms of a thiocarbonyl group, while in **4** only the C atom at the 2-position of a 1,3-diselenole ring has no AO coefficient. It should be noted that the AO coefficient albeit in very small amount appears at the S atom of a thiocarbonyl by substituting two Se atoms for two S atoms in a 1,3-dithiole ring.

Crystal Structures of 1·FeBr$_4$, and Two Plates (I and II) of 2$_2$·FeBr$_4$ and 2$_2$·GaBr$_4$. The molecule of **1** in **1**·FeBr$_4$ is actually in the **1**$^{+\bullet}$ state from the charge balance with the FeBr$_4^-$ counteranion. As shown in Figure 3, **1** is involved as a single crystallographically independent molecule in the crystal from a one-dimensional column. In each column, two neighboring molecules of **1** (**A**′ and **A**″) are tightly dimerized,

(26) Stewart, J. J. P. *MOPAC 2000*; Fujitsu Limited: Tokyo, Japan, 1999.

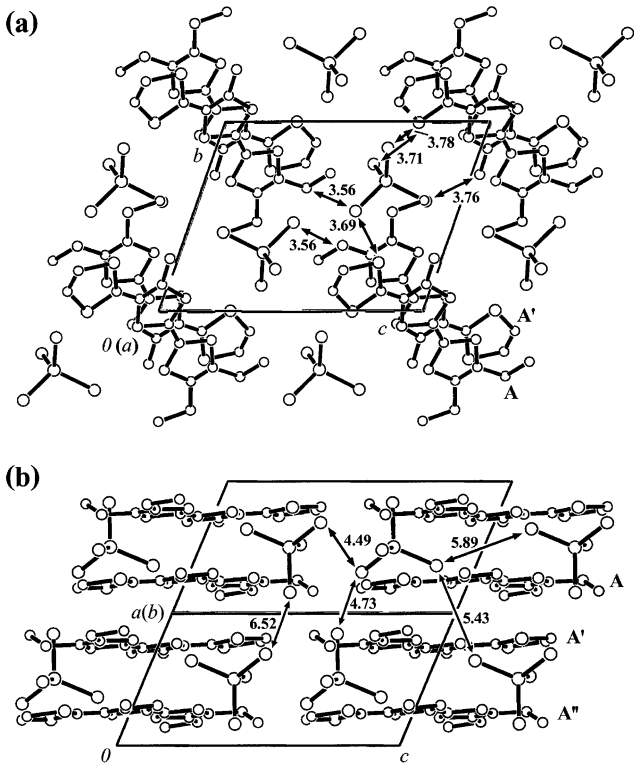

Figure 3. Crystal structure of **1**·FeBr$_4$: the views projected down the (a) *bc* and (b) (1̄10) planes.

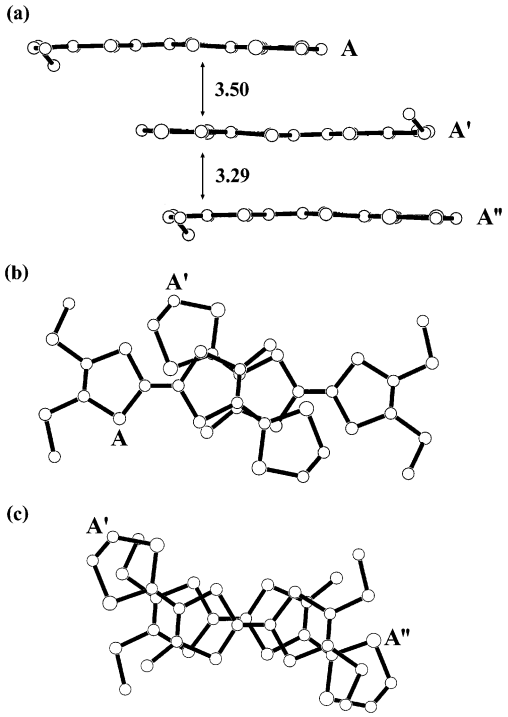

Figure 4. Stacking structure of molecules of **1** (**A**, **A**′, and **A**″) (a), and overlaps between **A** and **A**′ (b) and between **A**′ and **A**″ (c) in **1**·FeBr$_4$.

as seen from very short interplanar distance (3.29 Å) and effective overlap between them (see Figure 4). In contrast, the interdimer between **A** and **A**′ has a longer interplanar distance (3.50 Å) and very poor overlap. The **1** columns are aligned along the *a* axis to form two-dimensional (2D) layers. The FeBr$_4^-$ ions with a slightly distorted tetrahedral geometry

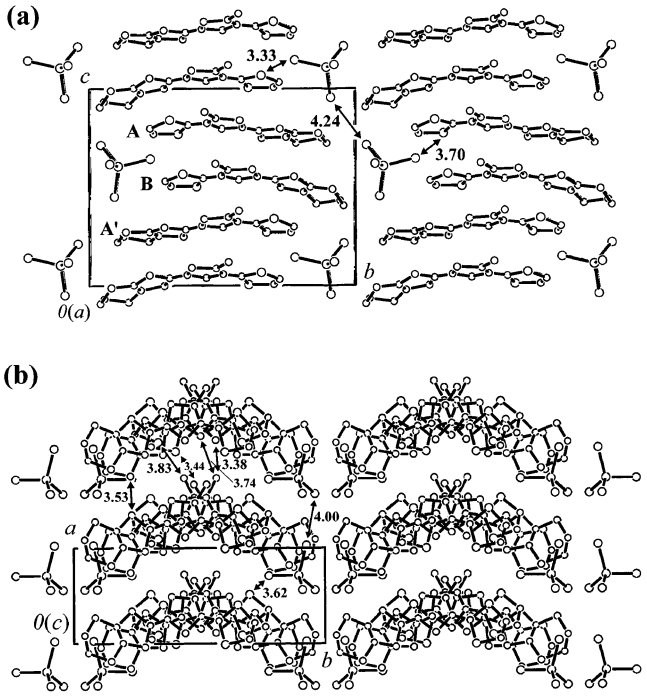

Figure 5. Crystal structure of $\mathbf{2}_2$·$FeBr_4$ (**I**): the views projected down the (a) *bc* and (b) *ab* planes.

around the Fe atom are located between the layers. The four Br atoms of the $FeBr_4^-$ ion have some short contacts (Br···S(Se) distance < the sum of van der Waals' radii of Br and S(Se) atoms, 3.80(3.95) Å[27]) with the S atoms of thiocarbonyl and methythio group and with the Se atom of 1,3-diselenole ring in **1**, but not with the four S atoms in the molecular backbone. All the Br···Br distances (4.49−6.52 Å) are somewhat longer than that (3.90 Å) of the van der Waals' contact.[27]

On the other hand, $\mathbf{2}_2$·$FeBr_4$ and $\mathbf{2}_2$·$GaBr_4$ have molecular formulas of two molecules of **2** and one $FeBr_4^-$ or $GaBr_4^-$ ion, so that each molecule of **2** is formally charged by $+^1/_2$ on the basis of the charge balance. Both $FeBr_4^-$ and $GaBr_4^-$ salts have two different crystal structures (**I** and **II**), respectively, but the crystal structures are almost the same between the $FeBr_4^-$ and $GaBr_4^-$ salts in the **I** or **II** crystals. Figure 5 shows the crystal structure of $\mathbf{2}_2$·$FeBr_4$ (**I**). The two crystallographically independent molecules of **2** (**A** and **B**) are involved in the crystal and stacked along the *c* axis in such a manner that **A** and **B** have an arrangement of molecules of **2** inverted to each other albeit maintaining their thiocarbonyl groups in the same direction, while **B** and **A′** have a similar arrangement albeit with slightly sliding the *b* axis to each other. The details in their overlaps between **A** and **B**, and between **B** and **A′**, can be well seen from Figure 6. Thus, the interplanar distances between **A** and **B**, and between **B** and **A′**, are the same and 3.46 Å, which is shorter than that of "π cloud thickness" (3.50 Å),[27] and the overlaps are fairly effective. As the result, the stacked columns composed of molecules of **2** have a structure like a half-cut pipe. Such stacked columns are aligned in the same direction

(27) Pauling, L. *The Nature of the Chemical Bond*, 3rd ed.; Cornell University Press: Ithaca, New York, 1960.

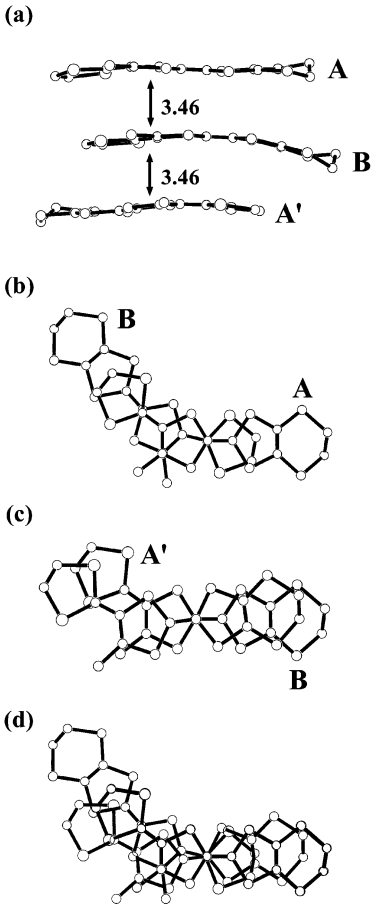

Figure 6. Stacking structure of molecules of **2** (**A**, **B**, and **A′**) (a), and overlaps between **A** and **B** (b), between **B** and **A′** (c), and between **A**, **B**, and **A′** (d) in $\mathbf{2}_2$·$FeBr_4$ (**I**).

along the *a* axis with several S···S contacts (the distances are shorter than that (3.90 Å) of the van der Waals' contact[27]) to form a 2D layer (see Figure 5b). In the case of **I**, these layers are arranged in the same direction along the *b* axis.

The $FeBr_4^-$ ions have a slightly distorted tetrahedral geometry around the Fe atom and are arranged in a zigzag manner between the layers composed of molecules of **2**. The distance between Br atoms of neighboring $FeBr_4^-$ ions in the *bc* plane is 4.24 Å, which is somewhat longer than 3.90 Å. However, there are two close contacts (the distances are 3.33 and 3.70 Å and shorter than that (3.95 Å) of the Br···Se van der Waals' contact[27]) between the Br atom of the $FeBr_4^-$ ion and the Se atom of a 1,3-diselenole ring in **2**. While, as far the $FeBr_4^-$ ions in the *ab* plane are concerned, the distance (4.00 Å) between the Br atoms is shorter than that in the *bc* plane. There is only one close contact (the distance is 3.62 Å) between the Br atom of the $FeBr_4^-$ ion and the Se atom of a 1,3-diselenole ring in **2**. The crystal structure of $\mathbf{2}_2$·$GaBr_4$ (**I**) is quite similar to that of the corresponding $FeBr_4^-$ salt, although there is a very small difference in the stacking structure of molecules of **2** and in the mutual arrangement of molecules of **2** and $GaBr_4^-$ or $FeBr_4^-$ ions between the two crystals.

The crystal structure of $\mathbf{2}_2$·$FeBr_4$ (**II**) is shown in Figure 7. In this crystal, the two crystallographically independent molecules of **2** (**A** and **B**) are also present and stacked along

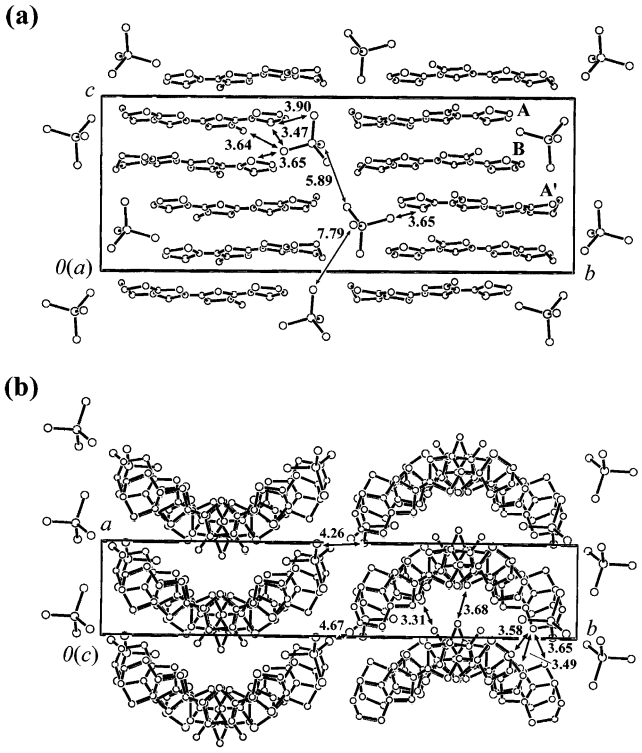

Figure 7. Crystal structure of $\mathbf{2}_2$·$FeBr_4$ (**II**): the views projected down the (a) *bc* and (b) *ab* planes.

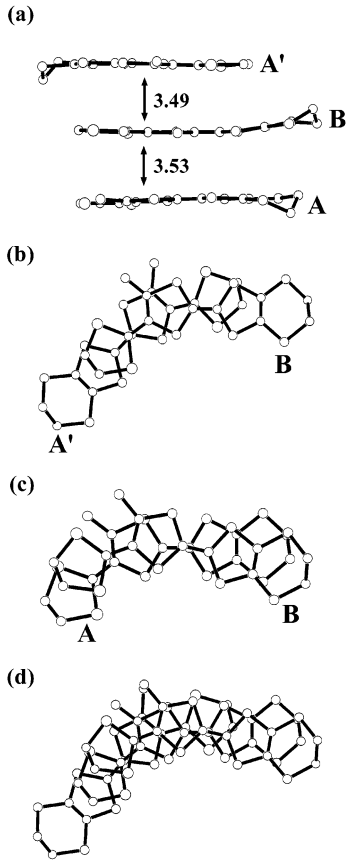

Figure 8. Stacking structure of molecules of **2** (**A**, **B** and **A′**) (a), and overlaps between **A** and **B** (b), between **B** and **A′** (c), and between **A**, **B** and **A′** (d) in $\mathbf{2}_2$·$FeBr_4$ (**II**).

the *c* axis in the manner similar to that in $\mathbf{2}_2$·$FeBr_4$(**I**). However, there is a slightly difference in the stacking structure between the two crystals (see Figure 8). The interplanar distances between **A** and **B**, and **B** and **A′**, are 3.49 and 3.53 Å, which are slightly longer than that (3.46 Å) in **I**. The overlaps between **A** and **B**, and between **B** and **A′**, are almost the same as those in **I**, although in the **B**/**A′** overlap the **A′** molecule slides by almost the same angles of 13° (**I**) and 15° (**II**) in the opposite direction to each other with respect to the **B** molecule (see Figures 6c and 8c). By such a **B**/**A′** overlap, the **2**-stacked column has a half-cut pipelike structure with a more regular and larger arc. The columns are also aligned in the same direction along the *a* axis. Several S···S contacts with shorter distances than 3.90 Å are present, forming a 2D layer. In marked contrast to the case of **I**, in **II** these layers have an alternately inverted arrangement along the *b* axis.

The $FeBr_4^-$ ions are also intervening between the layers, but as the result of a different layer arrangement as above the mutual arrangements between the neighboring $FeBr_4^-$ ions, and between the molecules of **2** and the $FeBr_4^-$ ions are changed. The shortest distance between the Br atoms of neighboring $FeBr_4^-$ ions in the *bc* plane becomes somewhat longer (5.89 Å) than that (4.24 Å) in **I**. While close contacts between molecules of **2** and $FeBr_4^-$ ions are increased, as shown by four close contacts with the distances 3.47, 3.65, 3.65, and 3.90 Å between the Br atoms of $FeBr_4^-$ ions and the Se atoms of molecules of **2**, and by one close contact with the distance of 3.64 Å between the Br atom of $FeBr_4^-$ ion and the S atom of a thiocarbonyl group in **2** molecule. In the neighboring $FeBr_4^-$ ions in the *ab* plane, the shortest distance between the Br atoms is 4.26 Å and becomes longer than that (4.00 Å) in **I**. The corresponding $GaBr_4^-$ salt has almost the same crystal structure as that of the $FeBr_4^-$ salt. However, a very small difference can be recognized in the stacking structure of molecules of **2** and in the mutual arrangement of neighboring counteranions as well as molecules of **2** and counteranions between the two crystals.

Electrical Conducting Properties. The room-temperature electrical conductivity on the single crystal of **1**·$FeBr_4$ was 1.9×10^{-3} S cm^{-1}. This low electrical conducting property is related to tight dimerization of the molecules of **1** charged by +1. In contrast, all of $\mathbf{2}_2$·$FeBr_4$ (**I**), $\mathbf{2}_2$·$GaBr_4$ (**I**), $\mathbf{2}_2$·$FeBr_4$ (**II**), and $\mathbf{2}_2$·$GaBr_4$ (**II**) showed fairly high electrical conductivities of 13.6, 8.9, 12.7, and 8.9 S cm^{-1} at room temperature, respectively. Figures 9 and 10 show the temperature dependences of resistivities (ρ's) for $\mathbf{2}_2$·$FeBr_4$ (**I**) and $\mathbf{2}_2$·$GaBr_4$ (**I**) between 5 and 300 K, and for $\mathbf{2}_2$·$FeBr_4$ (**II**) and $\mathbf{2}_2$·$GaBr_4$ (**II**) between 77 and 285 K, respectively. In the case of $\mathbf{2}_2$·$FeBr_4$ (**I**) and $\mathbf{2}_2$·$GaBr_4$ (**I**), such a $\rho-T$ behavior was observed such that ρ very slightly decreased with lowering the temperature from 300 or 285 K, and the decreasing trend continued until ca. 170 or 230 K, respectively. However, below the temperature, there was inversely an increase in ρ with lowering temperature, although both activation energies were very small, but different from each other (7 and 17 meV). These results suggest that the electrical conducting property is apparently metallic above ca. 170 or 230 K and semiconducting below the temperatures for the

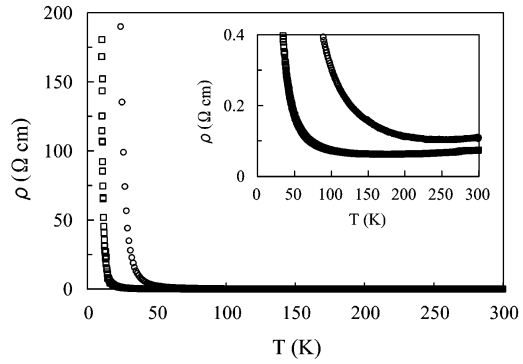

Figure 9. Temperature dependences of ρ's in (□) $\mathbf{2}_2$·$FeBr_4$ (**I**) and (○) $\mathbf{2}_2$·$GaBr_4$ (**I**) in the temperature range 5−300 K.

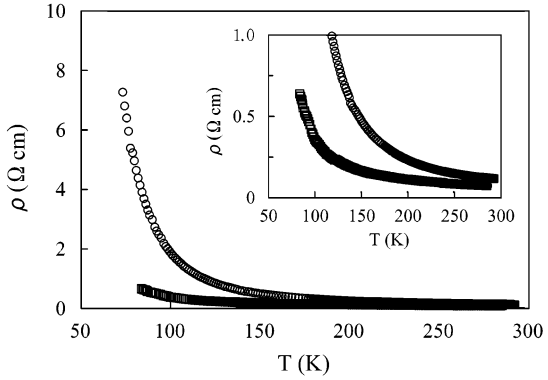

Figure 10. Temperature dependences of ρ's in (□) $\mathbf{2}_2$·$FeBr_4$ (**II**) and (○) $\mathbf{2}_2$·$GaBr_4$ (**II**) in the temperature range 77−285 K.

$FeBr_4^-$ and $GaBr_4^-$ salts, respectively. On the other hand, in the case of $\mathbf{2}_2$·$FeBr_4$ (**II**) and $\mathbf{2}_2$·$GaBr_4$ (**II**), both the salts exhibited semiconducting behavior between 77 and 285 K, but their activation energies were significantly different from each other in the measurements using several different samples, on average 21 meV for $\mathbf{2}_2$·$FeBr_4$ (**II**) and 38 meV for $\mathbf{2}_2$·$GaBr_4$ (**II**).

As the cause for markedly different electrical conducting properties in the $FeBr_4^-$ and $GaBr_4^-$ salts of **I** and also of **II**, two possible explanations are conceivable. The one is due to a significant difference in the stacking structures of molecules of **2** between the $FeBr_4^-$ and $GaBr_4^-$ salts, and the other is due to a somewhat π/d interaction in the $FeBr_4^-$ salt. As mentioned already, a significant difference can be not seen in the stacking structures of molecules of **2** between the $FeBr_4^-$ and $GaBr_4^-$ salts, so that the former possibility might be excluded. The latter possibility is very much probable, since the d spins of $FeBr_4^-$ ions seem to interact with each other with the aid of the conducting π electrons on the **2**-stacked columns, as discussed in the following Magnetic Properties section.

It is very rare that the electrical conducting properties are remarkably changed by different arrangements of **2**-stacked columns, i.e., metallic above 170 K and semiconducting below 170 K for the **I** crystals, while semiconducting in the whole temperature range for the **II** crystals. The different arrangement of **2**-stacked columns has significant influence on the stacking structure of molecules of **2** themselves, as is obvious from the interplanar distances and overlaps between the neighboring molecules of **2** in Figures 6 and 8. Thus, the interplanar distances between **A** and **B**, and between **B** and **A′**, for the **I** crystal are the same and 3.46 Å, which is shorter than the "π cloud" thickness.[27] On the other hand, the **II** crystal has different and longer interplanar distances of 3.49 Å between **A** and **B**, and 3.53 Å between **B** and **A′**. The overlaps between **A** and **B**, and between **B** and **A′**, as well as the contacts between the columns are almost the same between the **I** and **II** crystals. From a comparison of the two crystal structures, the **2**-stacked column for the **II** crystal can be regarded as a released form of the corresponding uniform and comparatively compact column for the **I** crystal. Since the **2**-stacked column is considered to be a main electrical conducting pathway, the different column structures are compatible with the metallic/semiconducting and semiconducting properties for the **I** and **II** crystals, respectively. In the future, it is necessary to investigate whether the electrical conducting property of the **II** crystal becomes close to that of the **I** crystal or not by the application of hydrostatic pressure.

ESR Spectra. The ESR spectra of $\mathbf{2}_2$·$GaBr_4$ (**I**) and $\mathbf{2}_2$·$GaBr_4$ (**II**) were measured at different temperatures between 3.6 and 300 K. These $GaBr_4^-$ salts only involve spins due to the conducting π electrons on the **2**-stacked columns, since the $GaBr_4^-$ ion is nonmagnetic. At 300 K, comparatively broad doublet signals were observed at $g = 2.0055$ (peak-to-peak width, $\Delta H_{pp} = 110$ Oe) for $\mathbf{2}_2$·$GaBr_4$ (**I**) and at $g = 2.0031$(158 Oe) for $\mathbf{2}_2$·$GaBr_4$ (**II**).[13,14] However, at 3.6 K, their signals became more sharp ($\Delta H_{pp} = 30$ Oe for $\mathbf{2}_2$·$GaBr_4$ (**I**) and $\Delta H_{pp} = 29$ Oe for $\mathbf{2}_2$·$GaBr_4$ (**II**)), but the g-values were almost not changed (2.0066 for $\mathbf{2}_2$·$GaBr_4$ (**I**) and 2.0082 for $\mathbf{2}_2$·$GaBr_4$ (**II**)). Now, the temperature dependences of g and ΔH_{pp} values were investigated, and the results are shown in Figure 11. For $\mathbf{2}_2$·$GaBr_4$ (**I**), the g-value was scarcely changed in the temperature range (see Figure 11a). On the other hand, a marked change was observed for the ΔH_{pp}, which was almost constant (100−110 Oe) between ca. 170 and 300 K but sharply decreased with lowering the temperature from ca. 170 K and again became almost constant (30−35 Oe) between ca. 30 and 3.6 K. (see Figure 11a). As shown in Figure 11b, the similar tendency was also obtained for $\mathbf{2}_2$·$GaBr_4$ (**II**), although there are some differences in the beginning of the decrease in the ΔH_{pp} at the higher temperature of ca. 200 K than ca. 170 K and in the larger decreased magnitude of ΔH_{pp} (ca. 130 Oe) than 80 Oe for $\mathbf{2}_2$·$GaBr_4$ (**I**), respectively. These results suggest that the conducting electrons are strongly correlated to each other in such a temperature region that the metallic and highly semiconducting properties are maintained, while, in the low semiconducting region, the electron correlation becomes smaller with lowering temperature.

On the other hand, the ESR spectra of $\mathbf{2}_2$·$FeBr_4$ (**I**) and $\mathbf{2}_2$·$FeBr_4$ (**II**) at 300 K showed only very broad doublet signals at $g = 2.0610$ ($\Delta H_{pp} = 1002$ Oe) and 2.0625 (939 Oe), respectively.[13,14] Of course, signals due to the conducting π electrons on the **2**-stacked columns as observed in $\mathbf{2}_2$·$GaBr_4$ (**I**) and $\mathbf{2}_2$·$GaBr_4$ (**II**) should also appear but will be hidden by the d signal because of weak intensity and broadness.

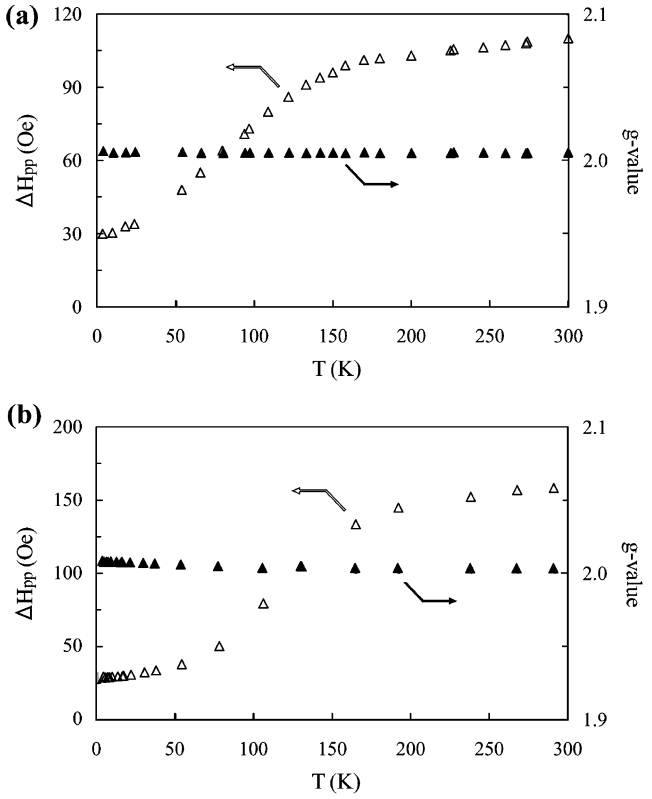

Figure 11. Temperature dependences of (▲) g-values and (△) ΔH_{pp}'s of doublet signals observed in the ESR spectra of microcrystals of (a) $\mathbf{2}_2$·$GaBr_4$ (**I**) and (b) $\mathbf{2}_2$·$GaBr_4$ (**II**).

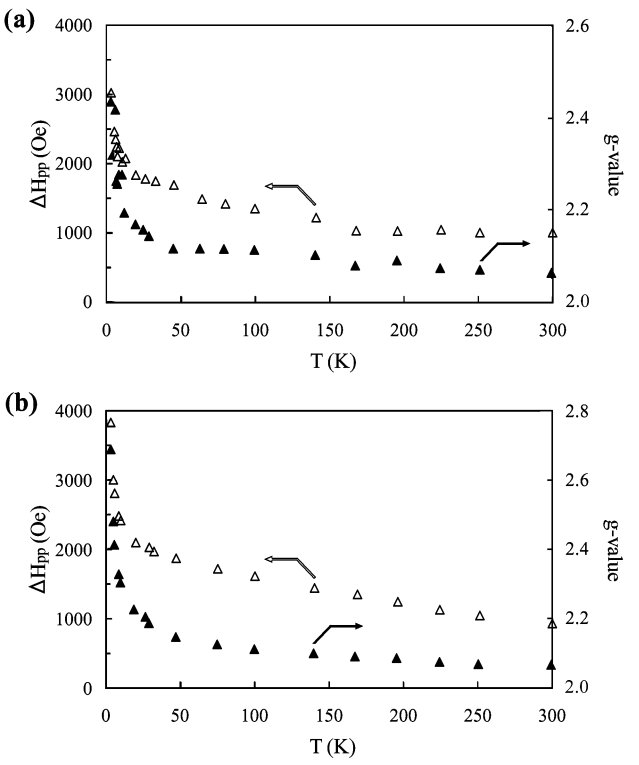

Figure 12. Temperature dependences of (▲) g-values and (△) ΔH_{pp}'s of doublet signals observed in the ESR spectra of microcrystals of (a) $\mathbf{2}_2$·$FeBr_4$ (**I**) and (b) $\mathbf{2}_2$·$FeBr_4$ (**II**).

With lowering the temperature from 300 K, the g and ΔH_{pp} values of the d signals gradually increased, and the degree of increase became remarkable below ca. 20 K, as shown from Figure 12: 2.4337 and 3025 Oe for $\mathbf{2}_2$·$FeBr_4$ (**I**), and 2.6887 and 3835 Oe for $\mathbf{2}_2$·$FeBr_4$ (**II**) at 3.2 K, the lowest temperature in this measurement. In contrast, for **1**·$FeBr_4$ very slight increase in the g-value and ΔH_{pp} was only observed with lowering the temperature from 300 to 3.2 K. These results suggest that the marked increase in the g-values and ΔH_{pp}'s below ca. 20 K for $\mathbf{2}_2$·$FeBr_4$ (**I**) and $\mathbf{2}_2$·$FeBr_4$ (**II**) reflects much more increased interaction between the $FeBr_4^-$ d spins leading to the antiferromagnetic ordering at lower temperatures, as mentioned in the next section in which the sharp decrease in the χ_p's occurs below 3.5 K for both $FeBr_4^-$ salts.

Magnetic Properties. Figure 13a shows the temperature dependences of χ_p and $\chi_p \cdot T$ in the temperature range 1.8−300 K for **1**·$FeBr_4$, $\mathbf{2}_2$·$FeBr_4$ (**I**), and $\mathbf{2}_2$·$FeBr_4$ (**II**), respectively. Since in all cases the $\chi_p \cdot T$ values gradually decrease with lowering the temperature from 300 K (see Figure 13b), antiferromagnetic interaction preferentially occurs between the d spins of $FeBr_4^-$ ions. Furthermore, as seen from Figure 13a, for $\mathbf{2}_2$·$FeBr_4$ (**I**) and $\mathbf{2}_2$·$FeBr_4$ (**II**) a sharp decrease in χ_p occurs below 3.5 K, where antiferromagnetic ordering might begin to take place. The $\chi_p - T$ behavior in the temperature range 5−300 K was analyzed by using the equation $\chi_p = C/(T - \theta) + \chi_\pi$, where C is a Curie constant and θ a Weiss temperature due to the d spins of $FeBr_4^-$ ions, and χ_p is a temperature-independent χ_p associated with the

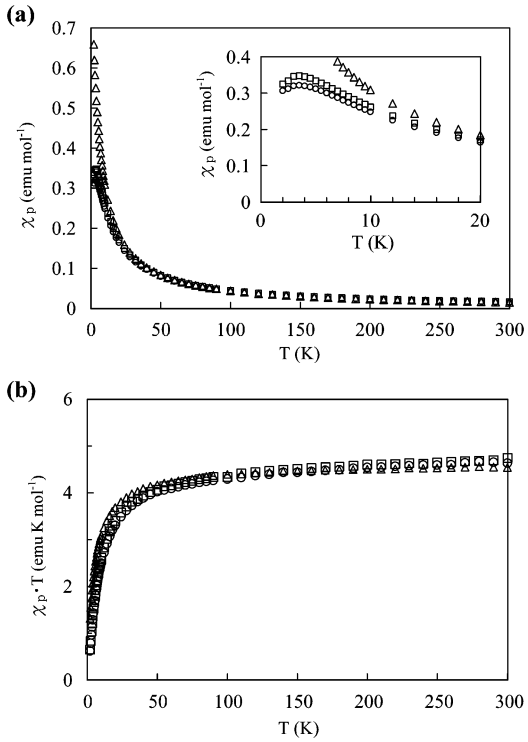

Figure 13. Temperature dependences of (a) χ_p and (b) $\chi_p \cdot T$ in the temperature range 1.8−300 K for (△) **1**·$FeBr_4$, (○) $\mathbf{2}_2$·$FeBr_4$ (**I**), and (□) $\mathbf{2}_2$·$FeBr_4$ (**II**).

conducting π electrons on the **1**- or **2**-stacked columns.[13,14] The best fit to the observed data was obtained by choosing the following C, θ, and χ_π values: $C = 4.60$ emu K mol^{-1}, $\theta = -5.3$ K, and $\chi_\pi = 0$ emu mol^{-1} for **1**·$FeBr_4$; $C = 4.53$

emu K mol^{-1}, $\theta = -7.3$ K, and $\chi_\pi = 8.0 \times 10^{-4}$ emu mol^{-1} for $\mathbf{2}_2$·$FeBr_4$ (**I**); $C = 4.58$ emu K mol^{-1}, $\theta = -6.7$ K, and $\chi_\pi = 8.0 \times 10^{-4}$ emu mol^{-1} for $\mathbf{2}_2$·$FeBr_4$ (**II**). All the C's obtained are close to the value (4.68 emu K mol^{-1}) calculated as an Fe(III) d spin entity with $S = {}^5/_2$ and $g = 2.069$. As for the θ's giving an important information on the nature of spin interaction, a small and negative value (−5.3 K) for **1**·$FeBr_4$ suggests that the d spins of $FeBr_4^-$ ions interact with each other in a very weak and antiferromagnetic manner, as supported by the fact that the neighboring $FeBr_4^-$ ions are remotely separated from each other (see Figure 3). The θ values (−7.3 and −6.7 K) for $\mathbf{2}_2$·$FeBr_4$ (**I**) and $\mathbf{2}_2$·$FeBr_4$ (**II**) are also negative and comparatively small, but unexpectedly larger as compared with that (−5.0 K) observed for the plate crystal of $\mathbf{5}_2$·$FeBr_4$[13] with a very similar arrangement of the $FeBr_4^-$ ions, which are located more closely than those for $\mathbf{2}_2$·$FeBr_4$ (**I**) and $\mathbf{2}_2$·$FeBr_4$ (**II**); i.e., the distances of Br atoms between the neighboring $FeBr_4^-$ ions are 3.70, 3.81, and 3.87 Å, values that are shorter than the values for the corresponding van der Waals' contact (3.90 Å)[27] for $\mathbf{5}_2$·$FeBr_4$, 4.00 and 4.24 Å for $\mathbf{2}_2$·$FeBr_4$ (**I**), and 4.26 and 5.89 Å for $\mathbf{2}_2$·$FeBr_4$ (**II**). This discrepancy can be reasonably understood by considering an indirect interaction between the d spins of $FeBr_4^-$ ions by the participation of S atoms in the 1,3-dithiole ring or Se atoms in the 1,3-diselenole ring. Thus, for $\mathbf{5}_2$·$FeBr_4$ there is only one short Br···S contact present with the shorter distance of 3.52 Å as compared to the corresponding van der Waals' contact (3.80 Å).[27] On the other hand, there are several closer Br···Se contacts with the distances of 3.33 and 3.70 Å for $\mathbf{2}_2$·$FeBr_4$ (**I**) and of 3.47, 3.65, 3.65, and 3.90 Å for $\mathbf{2}_2$·$FeBr_4$ (**II**), some of which are somewhat shorter than the van der Waals' Br···Se contact (3.95 Å).[27] Presumably, for the plate crystal of $\mathbf{5}_2$·$FeBr_4$, both direct and indirect interactions between the d spins of $FeBr_4^-$ ions are operative, while $\mathbf{2}_2$·$FeBr_4$ (**I**) and $\mathbf{2}_2$·$FeBr_4$ (**II**) prefer the indirect to the direct interaction.

Concluding Remarks

It is very interesting that in each case $\mathbf{2}_2$·$FeBr_4$ and $\mathbf{2}_2$·$GaBr_4$ of two different kinds of crystals, **I** and **II**, were obtained, both of which have similar crystal structures alternately aligned by **2**-stacked layers and $FeBr_4^-$ or $GaBr_4^-$ ion layers, except for all the same orientation of **2**-stacked layers in **I**, while there is laterally the opposite orientation of the layers in **II**. Such a different orientation exerted a significant influence on the stacking structure of molecules of **2** as well as on the relative arrangement of molecules of **2** and $FeBr_4^-$ or $GaBr_4^-$ ions between **I** and **II**. As the result, their electrical conducting properties on the **2**-stacked columns or layers, and also their interaction between the d spins of $FeBr_4^-$ ions, were different from each other.

In addition, it should be noted that both **I** and **II** crystals of $GaBr_4^-$ salts showed definitely different electrical conducting properties in the metal to semiconductor transition temperature ($GaBr_4^-$ salt, ca. 230 K and $FeBr_4^-$ salt, ca. 170 K) in **I** as well as in the magnitude of activation energies in the semiconducting region of **I** ($GaBr_4^-$ salt, ca. 17 meV and $FeBr_4^-$ salt, ca. 7 meV) and of **II** ($GaBr_4^-$ salt, ca. 38 meV and $FeBr_4^-$ salt, ca. 21 meV) from those of the corresponding $FeBr_4^-$ salts. This result suggests the presence of significant interaction between the conducting π electrons on **2**-stacked columns or layers and the d spins of the $FeBr_4^-$ ions and can also be supported by the crystal structure and magnetic properties results.

Since the donor molecules of **1** and **2** have a planar, but largely bent, molecular skeleton, it is of course expected that their electron densities in the ground state are markedly biased within the molecules, giving rise to large dipole moments. For example, the dipole moments of two crystallographically independent molecules of **2**, **A** and **B**, are calculated by a MOPAC method[26] to be 4.7−4.9 D and 4.3−4.6 D, respectively, which are slightly changed by the neutral or +1-charged species. If all the molecules of **2** are stacked with the same orientation in the 1D-manner and furthermore the 2D-manner, a very large dipole moment can be produced on the columns and layers of the crystals. Indeed, it is the case for the **I** and **II** crystals of $\mathbf{2}_2$·$FeBr_4$ and $\mathbf{2}_2$·$GaBr_4$, in which molecules of **2** are both arranged with the same orientation in each layer, although the layers have all the same orientation in **I**, while alternately the opposite orientation in **II**. The large dipole moment residing in each of the layers of **2** or in the whole crystal might have taken an important part in the different electrical conducting and magnetic properties between **I** and **II** crystals of $\mathbf{2}_2$·$FeBr_4$ and $\mathbf{2}_2$·$GaBr_4$ through the interaction with the conducting π electrons and/or the local d spins. We are now investigating such a possibility.

Acknowledgment. This work was in part supported by a Grant-in-Aid for Scientific Research on Priority Areas (B) (No. 11224209) from the Ministry of Education, Culture, Sports, Science, and Technology, Japan. We thank Dr. K. Takimiya and Prof. T. Otsubo (Hiroshima University) for supplying us 1,3-diselenole-2-selenone, and Dr. H. Fujiwara and Prof. H. Kobayashi (Institute for Molecular Science) for ESR measurements.

Supporting Information Available: X-ray crystallographic data in CIF format for **1**, **1**·$FeBr_4$, $\mathbf{2}_2$·$FeBr_4$ (**I**), $\mathbf{2}_2$·$FeBr_4$ (**II**), $\mathbf{2}_2$·$GaBr_4$ (**I**), and $\mathbf{2}_2$·$GaBr_4$ (**II**). This material is available free of charge via the Internet at http://pubs.acs.org.

IC030083V